Size Fractionation in a Phase-Separated Colloidal Fluid

Ben H. Erné,*,† Esther van den Pol,† Gert Jan Vroege,† Tom Visser,‡ and Henricus H. Wensink†

Van 't Hoff Laboratory for Physical and Colloid Chemistry and the Department of Inorganic Chemistry and Catalysis, Debye Institute, Utrecht University, 3584 CH Utrecht, The Netherlands

Received October 19, 2004. In Final Form: November 30, 2004

Phase separation of a polydisperse colloidal dispersion implies size fractionation. An application of this effect is given by size-selective purification procedures associated with the colloidal synthesis of so-called monodisperse nanoparticles. We used electron microscopy to determine detailed particle size distributions of coexisting colloidal fluid phases containing highly polydisperse iron oxide nanoparticles with a log-normal distribution ($\sigma = 0.54$ for the total system). Analysis of $N \approx 10000$ particles per phase yields the first five statistical moments of the distributions. Within experimental error, the interdependence of the statistical moments is in quantitative agreement with the "universal law of fractionation" proposed by Evans, Fairhurst, and Poon [*Phys. Rev. Lett.* **1998**, *81*, 1326], even though the theory was derived in the limit of slight polydispersity.

Introduction

Polydispersity is inherent to colloidal dispersions and affects their macroscopic physical properties, including the phase behavior. Since the individual colloidal particles are different from each other, the great number of degrees of freedom of the system enables the coexistence of arbitrarily many phases.[1] The coexisting phases have different particle size distributions than the overall system, but the distributions are intimately related. Evans, Fairhurst, and Poon[2,3] used thermodynamic perturbation theory to predict how the statistical moments of the distributions depend on each other. They also presented an experimental test of their theory,[2] largely based on model-dependent analysis of light scattering data, which does not give the most detailed information about the distributions. The theory was derived in the limit of slight polydispersity and gives important insight into size fractionation in phase-separated systems,[4] but the question remains how applicable it is to real systems, which are in general more than just slightly polydisperse. In particular, it can be asked whether the theory could be used to describe the size-selection procedures used in the preparation of nanoparticles with a polydispersity of 5% or less.[5−7] Here, we test the theory by analyzing a large number of individual particles in highly polydisperse coexisting colloidal fluid phases and in the single-phase system obtained after sufficient dilution.

The "universal law of fractionation" proposed by Evans, Fairhurst, and Poon[2,3] is independent of system parameters and therefore applies to any physical property of a slightly polydisperse system. For example, this can be the size of the particles in a colloidal fluid, the surface charge of such particles, or the length of polymer molecules in a polymer solution. The distribution parameter ϵ can be defined as follows for a property x:

$$\epsilon = [x - \langle x_P \rangle]/\langle x_P \rangle \quad (1)$$

where $\langle x_P \rangle$ is the average x in the total system; it is the average of the so-called "parent" system, present under single-phase conditions and different from the "daughter" phases obtained after phase separation. The ith moment of the distribution in one of the phases (parent or daughter) is given by

$$\langle \epsilon^i \rangle = \langle [(x - \langle x_P \rangle)/\langle x_P \rangle]^i \rangle \quad (2)$$

The first moment of the distribution, $\langle \epsilon \rangle$, corresponds to the average value relative to that of the parent distribution. The second moment, $\langle \epsilon^2 \rangle$, is closely related to the variance, given by $(\langle x^2 \rangle - \langle x \rangle^2)/\langle x \rangle^2$, and increases with the width of the distribution. The third moment, $\langle \epsilon^3 \rangle$, is nonzero when the part of the distribution below the average value of the parent distribution $\langle \epsilon_P \rangle$ does not exactly mirror the part of the distribution above $\langle \epsilon_P \rangle$. For the parent distribution, $\langle \epsilon^3 \rangle$ therefore describes the asymmetry or "skewness" of the function. In a simplified formulation, the theory[2] relates the difference between moments i and $i + 1$ of coexisting daughter distributions with moments $i + 1$ and $i + 2$ of the parent distribution:

$$\Delta\langle \epsilon^{i+1} \rangle / \Delta\langle \epsilon^i \rangle = \langle {\epsilon_P}^{i+2} \rangle / \langle {\epsilon_P}^{i+1} \rangle \quad (3)$$

For $i = 1$, the resulting mathematical expression,

$$\Delta\langle \epsilon^2 \rangle / \Delta\langle \epsilon \rangle = \langle {\epsilon_P}^3 \rangle / \langle {\epsilon_P}^2 \rangle \quad (4)$$

can be translated into words. Consider a single-phase system that separates into a bottom phase with mostly large particles and a top phase with mostly small particles (see Figure 1). The following trends are expected. A wide parent distribution ($\langle {\epsilon_P}^2 \rangle$) favors a large difference between the average values of the daughter distributions ($\Delta\langle \epsilon \rangle$).

* To whom correspondence should be addressed. E-mail: b.erne@chem.uu.nl.
† Van 't Hoff Laboratory for Physical and Colloid Chemistry.
‡ Department of Inorganic Chemistry and Catalysis.

(1) Sollich, P. *J. Phys.*: *Condens. Matter* **2002**, *14*, R79−R117.
(2) Evans, R. M. L.; Fairhurst, D. J.; Poon, W. C. K. *Phys. Rev. Lett.* **1998**, *81*, 1326.
(3) Evans, R. M. L. *Phys. Rev. E* **1999**, *59*, 3192.
(4) Fredrickson, G. H. *Nature* **1998**, *395*, 323.
(5) Murray, C. B.; Kagan, C. R.; Bawendi, M. G. *Annu. Rev. Mater. Sci.* **2000**, *30*, 545.
(6) Murray, C. B.; Sun, S.; Doyle, H.; Betley, T. *MRS Bull.* **2001**, Dec, 985.
(7) Hyeon, T. *Chem. Commun.* **2003**, 927.

10.1021/la047424h CCC: $30.25
Published on Web 01/20/2005

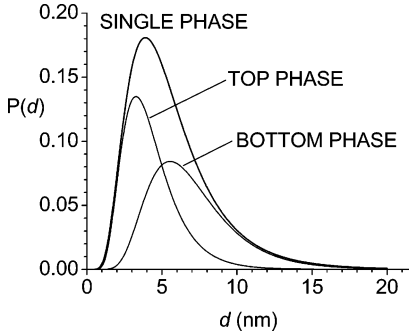

Figure 1. Sketch of log-normal top and bottom phase distributions that approximately add up to a normalized log-normal single-phase distribution (eq 5). The bottom phase clearly has a wider distribution than the top phase, due to the asymmetry of the single-phase distribution.

An asymmetrical parent distribution ($\langle\epsilon_P^3\rangle$) favors a large difference between the widths of the daughter distributions ($\Delta\langle\epsilon^2\rangle$). The consequence of these two trends is that the width difference between the daughter distributions is linearly dependent on the difference in their average values. The proportionality factor is determined by the shape of the parent distribution, that is, by the ratio of its skewness and its variance.

One consequence of the theory is that if the parent distribution is purely Gaussian (symmetrical, $\langle\epsilon_P^3\rangle = 0$), the daughter distributions will be the same and no size fractionation will occur. This is of practical importance in experimental systems.[4] To test the theory, the parent distribution should clearly be asymmetrical and detailed distribution functions should be determined both for the parent and the daughter systems. Our experimental approach is to choose a system with a wide log-normal distribution and to analyze a large number of particles in each phase using electron microscopy.

Experimental Section

The experimental system that we chose to test the theory was a colloidal dispersion of iron oxide nanoparticles (magnetite single crystals, Fe_3O_4) sterically stabilized by a surface layer of oleic acid molecules and dispersed in the organic solvent toluene. Due to the chemical precipitation method used to make the particles,[8] they are highly polydisperse and asymmetrically distributed in favor of the smallest particles, approximately according to a log-normal distribution:

$$P(d) = [\sigma d(2\pi)^{1/2}]^{-1} \exp[-(\ln d - \ln d_0)^2/(2\sigma^2)] \qquad (5)$$

where d is the diameter, σ^2 is the variance, and d_0 is the central value of the distribution when plotted with a logarithmic horizontal axis. An advantage of our chemical system is that the particles are small (average diameter $\approx$ 7 nm), so that a great number of particles can be imaged simultaneously by electron microscopy. Moreover, they are stable in the electron microscope, with its powerful electron beam and ultrahigh vacuum, and they offer a high image contrast.

The particles were sufficiently small that magnetic interactions were negligible compared to the thermal energy, in the absence of an applied magnetic field (in the presence of a strong magnetic field, the system behaves as a ferrofluid[9]). Phase separation was obtained by adding nonadsorbing polymer, poly(dimethylsiloxane) (PDMS, 41.5 kg mol^{-1}), which results in depletion attraction between the colloids.[10,11] The radius of gyration of the polymer was 8.5 nm, even larger than the diameter of most magnetite particles, so that phase separation was easily obtained at concentrations above the overlap concentration of 27 g L^{-1}. Phase separation was studied earlier in exactly the same system, and complicated features of the magnetic measurements were ascribed to size fractionation.[12]

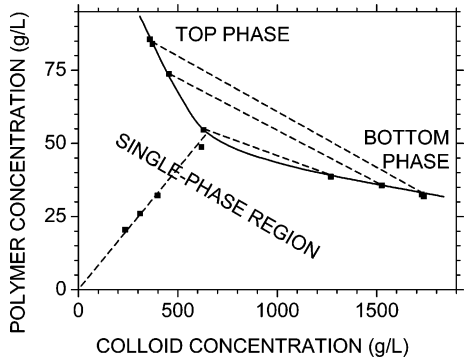

Figure 2. Experimental phase diagram for the investigated system consisting of polydisperse Fe_3O_4 colloidal particles and nonadsorbing PDMS polymer molecules in toluene. It is the first time that such a diagram was obtained by height-resolved in situ infrared spectroscopy (ref 13). The curve is the approximate binodal, and the tie lines indicate the composition of coexisting phases, consisting of a colloid-rich bottom phase and a polymer-rich top phase. Due to polydispersity, the binodal curve would be different for a different slope of the dilution line than that shown here in the single-phase region (ref 1).

An experimental phase diagram of the system at 20 °C is shown in Figure 2. It gives the polymer and colloid concentrations above which phase separation occurred. The bottom phase is a colloidal liquid phase, with a high density due to a high colloid concentration, and the top phase is a colloidal gas phase, with a lower density and colloid concentration. A colloid concentration of 1000 g L^{-1} corresponds to a volume fraction of about 0.3. The diagram was obtained by height-resolved in situ infrared spectroscopy.[13] With this technique, the concentrations of both components, the polymer and the colloid, are separately analyzed in both coexisting phases under equilibrium conditions. It was verified that the absorbance was linear with the concentration for all chemical contributions to the infrared spectrum. The convenient but indirect method to determine phase diagrams by Bodnár and Oosterbaan[14] could not be used here because it assumes monodispersity of the particles. Size fractionation means that there is no unique phase diagram. The lever rule does not hold, and the location of the binodal curve depends on the slope of the dilution line.[1]

Particle size distributions corresponding to the points in Figure 2 were obtained in the following way. First, the most concentrated coexisting phases were analyzed by in situ infrared spectroscopy,[13] after which samples were taken for electron microscopy and solvent was added to obtain less concentrated coexisting or single phases. Each time, the system was given 16 h to equilibrate. This equilibration time was sufficient to attain a steady state, judging from height profiles of the magnetic susceptibility measured in parallel with the infrared measurements using a setup described earlier.[15] These profiles showed a sharp phase boundary (an infrared height profile of this system is reported in ref 13). The lack of magnetic aggregates in all the fluid phases was verified by measuring the frequency dependence of the magnetic susceptibility;[15] the imaginary component was always negligible and the real component frequency independent, at least below 100 kHz. Samples for electron microscopy were taken using a syringe, first from the top phase and then from the still undisturbed bottom phase. Copper grids were used that had holes of 10 μm by 10 μm covered by a thin organic film (Formvar) with

(8) Bica, D. *Rom. Rep. Phys.* **1995**, *47*, 265.
(9) Rosensweig, R. E. *Ferrohydrodynamics*; Cambridge University Press: Cambridge, 1985.
(10) Asakura, S.; Oosawa, F. *J. Chem. Phys.* **1954**, *22*, 1255.
(11) Vrij, A. *Pure Appl. Chem.* **1976**, *48*, 471.
(12) Van Ewijk, G. A.; Vroege, G. J.; Kuipers, B. W. M. *Langmuir* **2002**, *18*, 382.
(13) Erné, B. H.; Van der Maas, J. H.; Kuipers, B. W. M.; Visser, T.; Philipse, A. P. *Langmuir* **2003**, *19*, 3081.
(14) Bodnár, I.; Oosterbaan, W. D. *J. Chem. Phys.* **1997**, *106*, 7777.
(15) Erné, B. H.; Butter, K.; Kuipers, B. W. M.; Vroege, G. J. *Langmuir* **2003**, *19*, 8218.

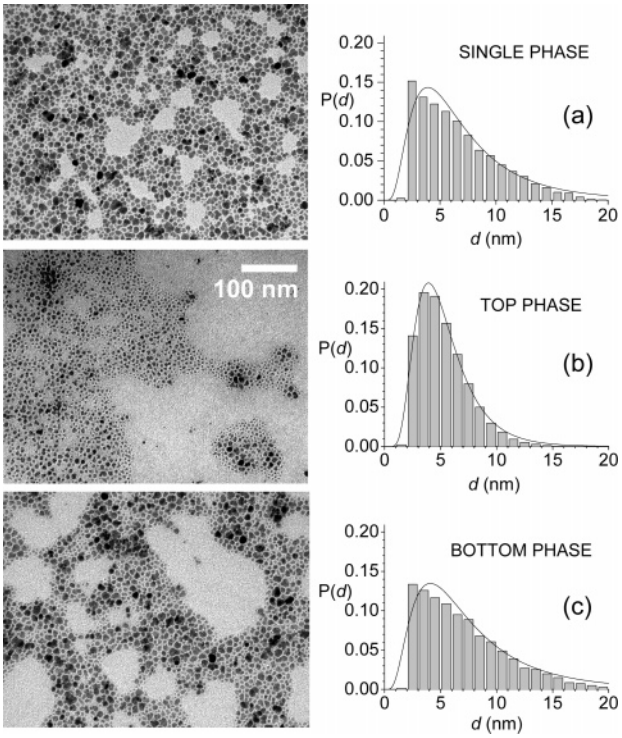

Figure 3. Transmission electron microscopy and statistical size analysis of (a) the single-phase system and (b,c) the two coexisting phases with the highest overall concentration in Figure 2. All three images are on the same scale. The curves are log-normal fits of the data (eq 5).

graphite nanoparticles to enhance its electrical conductivity, and the grids were simply dipped into the samples obtained with the syringe after they had been strongly diluted. Images were obtained using a Philips Tecnai10 at 80 kV. Electronic image files were obtained with hundreds of particles per picture, each pixel having its own gray value and corresponding to about 0.5 nm by 0.5 nm. Particle size distributions were determined by analyzing 8000−16000 particles per phase using image analysis computer software.[16]

Results and Discussion

Figure 3 shows images and normalized particle diameter distributions of the most concentrated coexisting phases and of the single-phase system obtained after sufficient dilution. The largest particles (dark spots) are clearly found in the bottom phase, as expected, because the density of bulk magnetite is higher than that of the solvent. The background gray value is relatively homogeneous, so that it could be subtracted with sufficient reliability. The particles are mostly present in a partial monolayer and could therefore be analyzed separately (areas with particles that were on top of each other were left out of the analysis). The distance between neighboring particles is relatively homogeneous because it is determined by the thickness of the organic layer at the surface of the particles, consisting of a monolayer of (monodisperse) oleic acid molecules. The space between adjacent particles looks empty, since the oleic acid molecules are practically transparent to the electron beam, and the distance between adjacent particles is about 4 nm, sufficient to judge adjacent particles as distinct. The top phase not only has a smaller average particle size, but also a narrower and more symmetrical distribution than the bottom phase, that closely resembles the single-phase system. Upon dilution, the differences between the coexisting phase distributions gradually disappear.

(16) AnalySIS Pro software, version 3.2; Soft Imaging Systems GmbH: Münster, Germany (copyright 1986−2002).

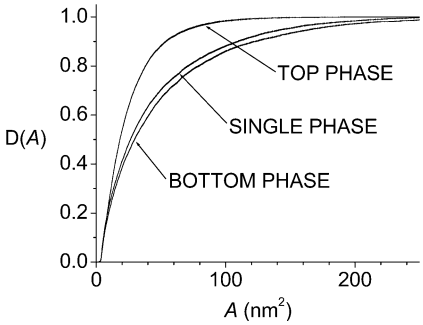

Figure 4. Experimental cumulative distributions D of the cross-sectional surface area A of the particles in the single, top, and bottom phases also shown in Figure 3. The plotted points are the raw data, without any fitting or correction.

The large difference in particle size distribution between the two phases is also evidenced by other observations. The infrared spectra not only give the concentration of magnetite in each phase but also the amount of oleic acid molecules adsorbed at the surface of the magnetite particles,[13] and this indicates that the surface-to-volume ratio was roughly twice as high in the top phase as in the bottom phase, as expected from the smaller particle size measured by electron microscopy. The magnetic measurements are also affected by size fractionation. The most concentrated bottom phase has an initial magnetic susceptibility of 3.5 compared to 0.03 for the coexisting dilute phase, even though there is only a factor of 5 between the weight concentrations of the two phases; this large difference can be understood from the fact that the initial magnetic susceptibility strongly depends on the magnetic radius of the particles.[15]

The histograms in Figure 3 show practically no particles below $d = 2$ nm. The image analysis disregards those particles because they are difficult to separate from the background noise and the graphite nanoparticles of the organic thin film below the particles. Moreover, larger particles are more reliably analyzed than smaller particles, because larger particles are thicker and therefore darker. These limitations of the analysis are arguments to give a higher weight to larger particles during statistical analysis of the data. This can be done by analyzing not the particle diameters d but the cross-sectional surface areas A. A more fundamental reason for analyzing surface areas is that the raw data consist of a number of pixels per particle, about 4 pixels per nm^2, whereas the diameters d given by the image analysis software are derived from such data, on the assumption that $A = (\pi/4)d^2$, even though the particles are potato-shaped rather than spherical. We will therefore test the size fractionation theory on measured distributions of the cross-sectional surface area of the particles, without making an assumption about the shape of the particles.

Figure 4 shows the cumulative distributions for the cross-sectional surface area in the single, top, and bottom phases also presented in Figure 3. Again, the difference between top and bottom phases is pronounced, whereas the difference between the bottom and single phases is much more subtle. In line with Figure 3, a cutoff is clearly visible around $A \approx 3$ nm^2. By adding a few percent of hypothetical smaller particles, distributions can be obtained that are in excellent agreement with a log-normal distribution, but such a "correction" will not be implemented here, because of its somewhat arbitrary nature.

In Figure 5, the particle distributions from electron microscopy are plotted according to eq 3 for $i = 1-3$, with

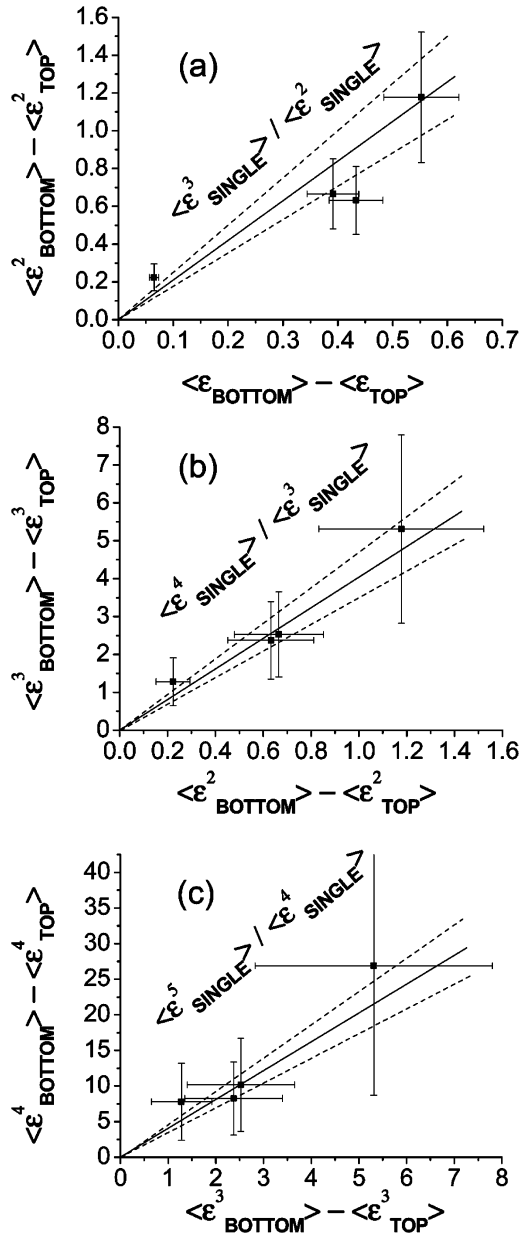

Figure 5. Statistical analysis of size fractionation in the system of Figures 2−4 according to the theory of Evans, Fairhurst, and Poon (refs 2 and 3) (eq 3). The property x in eqs 1 and 2 is the cross-sectional surface area A of the particles determined from electron microscopy. The full lines are not fits of the data but indicate the theoretical slope calculated on the basis of the single-phase distribution, and the dotted lines give the error in the calculated slopes. The calculation of the errors is discussed in the text.

x in eqs 1 and 2 being the cross-sectional surface area A (the quality of the data does not allow going further than $i = 3$). The lines going through the points are not data fits but give the theoretically predicted slope according to eq 3. Within experimental error, the measured particle size distributions are in quantitative agreement with the size fractionation theory by Evans, Fairhurst, and Poon.[2,3]

The error bars and the errors in the predicted slopes in Figure 5 were calculated in an unconventional way. The statistical error s_x in the measurement of a single particle is not responsible for the error bars, since on that basis, the errors in the statistical moments would be negligible on the scales of Figure 5. For instance, the error in the average value of the parent distribution is of the order of $s_x N^{-1/2}$, where s_x is about 1 nm for the diameter and $N \approx 10000$ is the number of measured particles. Nevertheless, the scatter of the points in Figure 5 suggests the presence of errors of the order of 10−20%. These are probably systematic errors in obtaining and analyzing images of the particles, errors that could even be different from one image to another. Two sources of systematic error are the finite resolution of the images (which broadens the particles) and limitations of the image analysis procedure, by which particle edges are truncated and particles below 2 nm are disregarded. To estimate the effect of such systematic errors, we repeated the statistical analysis of the raw data after adding 1 nm to the measured diameter of each particle (or if one prefers, a 1 nm ring was added to the surface area of each particle). This led to one extremity of the error bars in Figure 5. We also repeated the statistical analysis of the raw data after subtracting 1 nm from the measured diameter of each particle, leading to the other extremity of the error bars in Figure 5.

The advantage of our colloidal system is the relative ease with which a great number of particles could be analyzed. However, it is clearly a drawback that a systematic error of only 1 nm may dominate all other sources of error. In principle, an even better system to test the theory using microscopy would have larger particles compared with the resolution of the microscope, to decrease systematic errors. Moreover, the number of particles analyzed could probably go down significantly before statistical errors start to outweigh the systematic errors.

Conclusion

Figure 5 indicates that the size fractionation theory by Evans, Fairhurst, and Poon[2,3] for slightly polydisperse systems can also hold for a system with a broad distribution. This suggests that the theory is applicable to a wide range of colloidal systems, since colloidal synthesis often automatically leads to particles with a broad log-normal distribution, comparable to the system studied here. Size fractionation of particles obtained by colloidal synthesis is of great importance in the preparation of so-called monodisperse nanoparticles. If the particles are to self-assemble into superlattices, the standard deviation in particle size must be 5% or less, whereas a one-step colloidal synthesis often yields a polydispersity that is higher. Size-selective purification steps are therefore standard procedure in the preparation of such particles.[5−7] One approach is to precipitate out the largest particles by adding a lower quality solvent and centrifuging. Our results with highly polydisperse nanoparticles suggest that the tested size fractionation theory holds for such systems and could therefore be used to guide the improvement of the size-selection procedures.

Acknowledgment. We thank J. H. Meeldijk and A. van Blaaderen for a helpful discussion and B. W. M. Kuipers for automating the height-dependent magnetic susceptibility measurements.

LA047424H